

FLUID INCLUSION EVIDENCE FOR THE GENESIS OF THE MOUNT BRUSSILOF MAGNESITE DEPOSIT, BC, CANADA

By Dan Marshall, Simon Fraser University, Burnaby, BC, Canada
George Simandl, British Columbia Geological Survey, Victoria, BC, Canada
and Danae Voormeij, University of Victoria, Victoria, BC, Canada
marshall@sfu.ca

ABSTRACT

The depositional environment of carbonates hosting the Mt. Brussilof deposit supports evaporitic origin for magnesite but it does not preclude either late diagenetic or hydrothermal origin. Textural evidence indicates either diagenetic recrystallization of sedimentary magnesite precursors or hydrothermal origin for the magnesite ores. Fluid inclusion studies reveal involvement of two independent but coeval fluids. One fluid inclusion population, found in quartz growth zones, is a CO₂-bearing saline brine represented by three-phase fluid inclusions. The other population found in magnesite and dolomite veins, is represented at room temperature by two-phase brine inclusions containing no CO₂. Petrographic work indicates that both fluid inclusion populations coexisted at the temperatures and pressures of fluid inclusion trapping. The intersection of the two isochoric constraints from the coeval fluid generations is consistent with maximum formational temperatures between 195 to 305°C and maximum pressures of approximately 2650 bars, corresponding to burial depths on the order of 8 km. This study is consistent with sedimentary/diagenetic formation of magnesite followed by a relatively minor hydrothermal overprint. Vein-forming carbonates, mainly sparry dolomite with minor magnesite are part of the hydrothermal overprint.

INTRODUCTION

There are a number of large, sedimentary-hosted, potentially economic magnesite deposits in British Columbia (Simandl and Hancock, 1996; Simandl, 2002). Only one of these, the Mount Brussilof mine (owned by Baymag Inc.), is currently in production. The mine is located in the southeastern part of the province, approximately 35 kilometres northeast of Radium Hotsprings, within the Foreland tectonostratigraphic belt and Kicking Horse Rim. The western margin of the Kicking Horse Rim coincides with the Cathedral paleoescarpment (Figure 1) along which there are a number of magnesite and Mississippi Valley Pb-Zn showings (Simandl and Hancock, 1991). The rocks within the pit consist mainly of light coloured, nearly monomineralic, coarse textured magnesite ore (Figures 2, 3, and 4). Gangue minerals are either disseminated within magnesite, fracture related or found as open space fillings (Simandl and Hancock, 1999).

Three genetic models are commonly suggested to explain the origin of sparry magnesite deposits (Simandl

and Hancock, 1999). These are: replacement of dolomitized, permeable carbonates by magnesite due to interaction with a hydrothermal fluid (Lugli *et al.*, 2000; Singh and Sharma, 1997; Kralik and Hoefs, 1978, Morteani *et al.*, 1982; Aharon, 1988, Simandl *et al.*,

1991); diagenetic recrystallization of a magnesia rich protolith deposited as a chemical precipitate in marine or lacustrine settings (Fritz and Simandl, 1993; Pohl, 1990; Pohl and Siegl, 1986) and direct precipitation from hydrothermal fluids (Fallick *et al.*, 1991; Halfon and Marcé, 1975). Field and macroscopic textural observations at the Mount Brussilof deposit indicate that in most cases, magnesite textures can be interpreted as late diagenetic replacement or as hydrothermal in origin. Structural and stratigraphic settings are described in the section on regional geology suggest sedimentary origin for the magnesite protolith. It is likely that the primary sediments consisted of fine-grained magnesite, hydromagnesite, huntite or other low temperature magnesia-bearing minerals and that these minerals recrystallized or were converted into magnesite during the late diagenesis.

REGIONAL GEOLOGY

The Mt. Brussilof deposit is hosted within the Middle Cambrian Cathedral Formation (Figure 1). The Cathedral formation is approximately 340 metres in thickness and is comprised of white, grey and buff coloured limestone and dolomite with minor quartz and pyrite veins and disseminations (Simandl and Hancock, 1991). The Cathedral conformably overlies the Naiset formation (Figure 5). Conformably overlying the

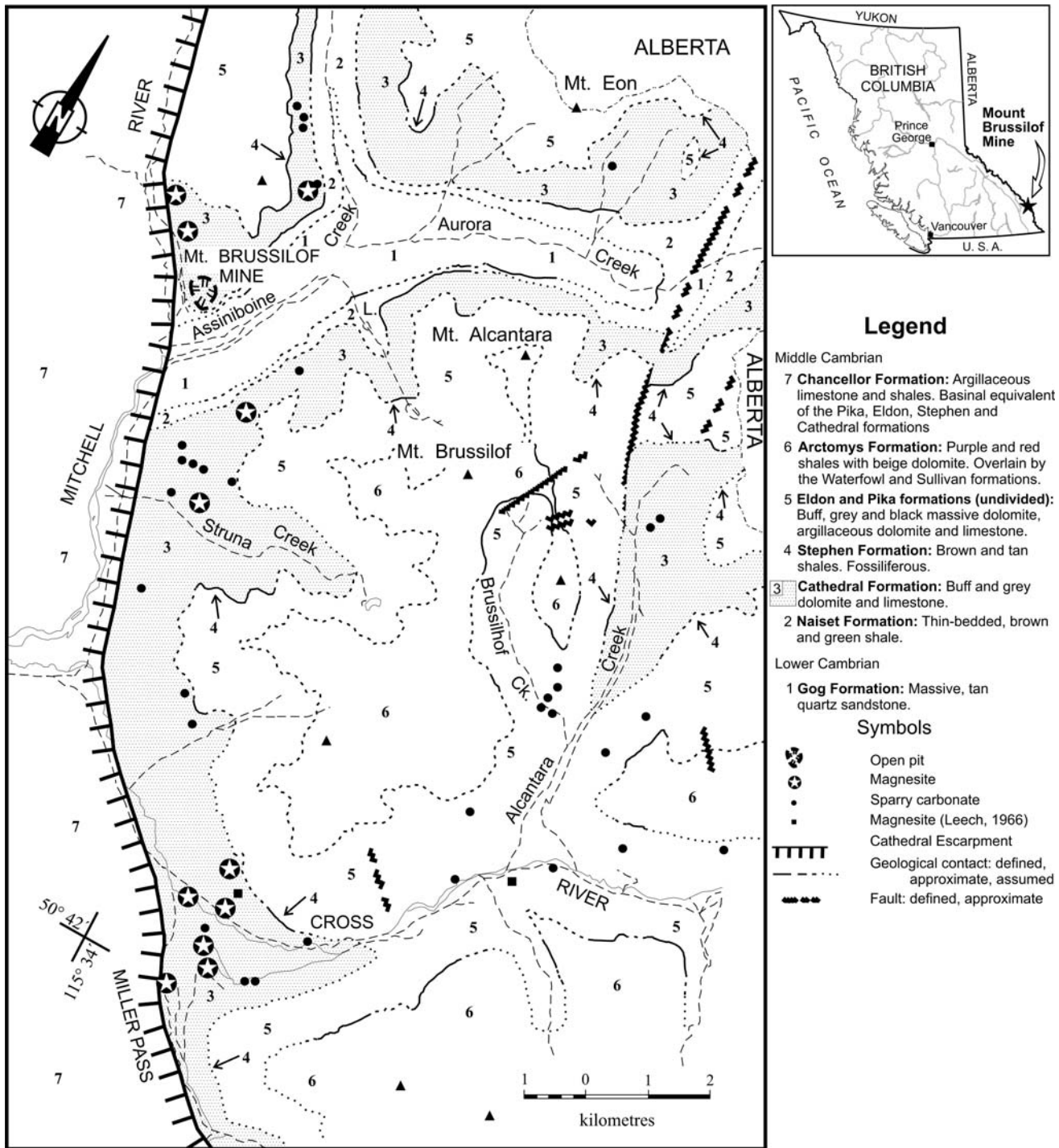


Figure 1. Geology map of the Mount Brussilof area, showing the location of the Mount Brussilof mine and other magnesite deposits in general proximity to the Cathedral paleoescarpment and Kicking Horse Rim (after Simandl, 1991).

Cathedral Formation are the Middle Cambrian Stephen, Eldon, Pika, Actomys and Chancellor formations. Rock types in these formations vary from shales and argillites to limestones, and are locally fossiliferous. The entire Middle Cambrian succession unconformably overlies Lower Cambrian massive quartz sandstones of the Gog Formation. Rocks outcropping west of the Cathedral Escarpment (Figure 1) are strongly deformed, but those to the east are not (Simandl *et al.*, 1991). The Cathedral, Eldon, and Pika formations have poorly developed cleavage, while the rocks of the Stephen and Naiset Formations have well developed foliation. In Mount Brussilof area, magnesite showings are restricted to the Cathedral Formation and up to now, magnesite has not been found west of the Cathedral escarpment (Figure 1). Fine-grained dolostone and late sparry dolomite are present on both sides of the Cathedral Escarpment (Simandl *et al.*, 1991). The magnesite host rocks are carbonates of the Cambrian Cathedral Formation, which were deposited in a relatively shallow marine environment (Fritz and Simandl, 1993). Where the field relationship between sparry dolomite and sparry magnesite is clear: the sparry dolomite appears younger than sparry magnesite.

This study is based upon fluid inclusions, field and microscope observations. The veins and other open space fillings sampled and studied consist of dolomite, magnesite and quartz (Figure 6). The veins show no evidence of deformation. Vein width varies from centimetres up to tens of centimetres. Dolomite is the dominant vein mineral, but in thin sections, in most cases, it is difficult to distinguish between dolomite and magnesite without an electron microscope or microprobe. The majority of crystals within the veins are idiomorphic and range in size from few millimeters to several centimeters in length. In some cases the carbonates and quartz crystals show growth zones. Fluid inclusions from within selected growth-zoned crystals have been examined and analyzed in detail (Figure 7). In a few cases magnesite has been observed as overgrowths on existing dolomite crystals. That particular paragenesis was not previously observed at Mount Brussilof.

Fluid Inclusion Data:

Samples of typical magnesite ore were not studied because fluid inclusions that they contained were too small (less than 5 microns in diameter). The four samples studied for fluid inclusions are from the late quartz-carbonate veins. Two samples are zoned quartz crystals and the other two samples are carbonate samples from the vein. One carbonate sample is a clear crystal of magnesite. The other carbonate sample is a composite sample taken from the vein wall. It consists of a cloudy sparry dolomite overgrown by a clear

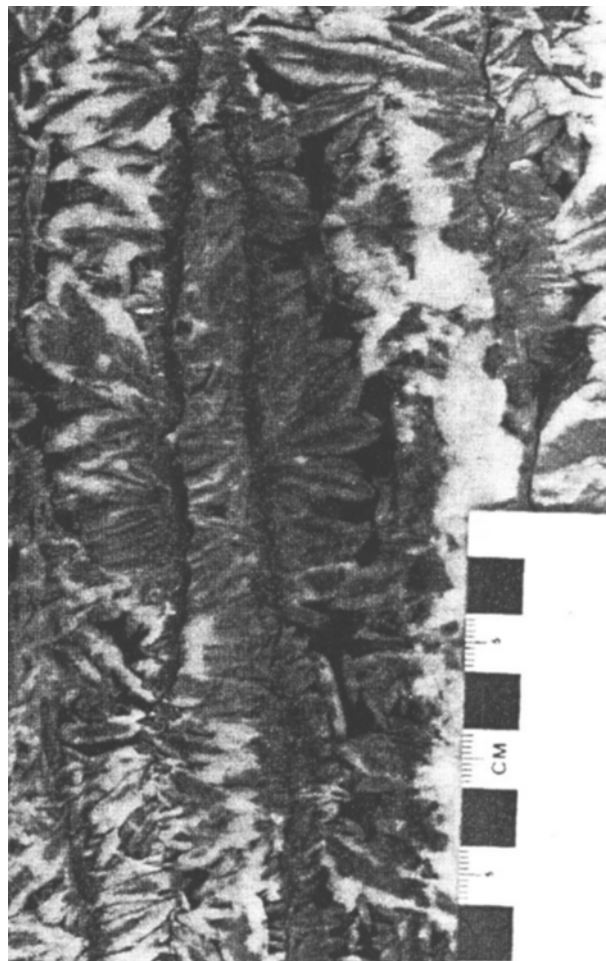


Figure 2. Zebra banding in magnesite, vestigial silty dolomitic protolith (black) with zoned magnesite crystals (white and light grey).

magnesite rim. Drusy quartz (Table 1) hosts Type 1 three-phase fluid primary inclusions that range up to 120 micrometres across with variable shapes. These inclusions occur within healed fractures, as isolated inclusions, and along growth zones. The contained phases are an aqueous phase, a liquid carbonic phase, and a vapour carbonic phase. At room temperature the carbonic vapour and carbonic liquid phases occupy approximately 7 and 1 percent, respectively, of the inclusion volume. When these inclusions are cooled, they nucleate a clathrate at an average temperature of -31°C followed closely by the nucleation of ice at approximately -35°C . Continued cooling results in nucleation of solid CO_2 at approximately -90°C . No additional phases nucleated when samples were further cooled to -195°C . Subsequent warming of the fluid inclusions causes the solid CO_2 to melt at temperatures near the CO_2 triple point (-56.6°C). Continued heating resulted in the melting of ice at temperatures above -29°C ; with final ice melting temperatures in the range of -8.5 to -3.5°C . Clathrate melting (Figure 8) takes place over the temperature interval from 7.5 to 8.9°C .



Figure 3. Stylolite-like fractures, with pyrite and calcite. Recrystallized pyrite and calcite along the stylolites is indicative of fluid flow. 1-dollar coin for scale.

SAMPLE DESCRIPTIONS

Homogenization of the carbonic phases to carbonic vapour occurs in the temperature interval 28.2 to 29.8°C. Total homogenization to the liquid occurs over the temperature range 190 to 210°C. These data are consistent with fluid compositions of $X\text{-CO}_2 = 0.010$, $X\text{-H}_2\text{O} = 0.975$ to 0.983 and $X\text{-NaCl} = 0.007$ to 0.015 (2.2 to 4.8 wt% NaCl equivalent). Raman microprobe analyses of the carbonic phases of these inclusions indicate that N_2 , CH_4 and H_2S concentrations are below the detection limit.

Inclusions in the magnesite (Table 2) are mainly two-phase fluid (Type 2) with rare three phase fluid inclusions (Type 1). The dominant two-phase fluid inclusions (Type 2) are comprised of a vapour and an aqueous phase. The vapour phase occupies

approximately 10 % of the inclusion volume at room temperature. Upon cooling, these inclusions nucleate ice at approximately -45°C. Further cooling to -195°C does not cause any additional phases to nucleate. Upon heating, the ice begins to melt at temperatures above -30°C, with the final disappearance at temperatures in the range of -4 to -5°C (Figure 9). Further heating results in a continual decrease in the size of the vapour bubble until total homogenization occurs at temperatures of 170 to 190°C. Many of the larger fluid inclusions decrepitate or stretch upon heating. To obtain reliable measurements, we concentrated on a number of smaller inclusions with similar phase ratios that were located away from the polished surfaces and defects within the magnesite. These microthermometric data correspond to compositional ranges of 6.4 to 7.8 wt% NaCl equivalent.

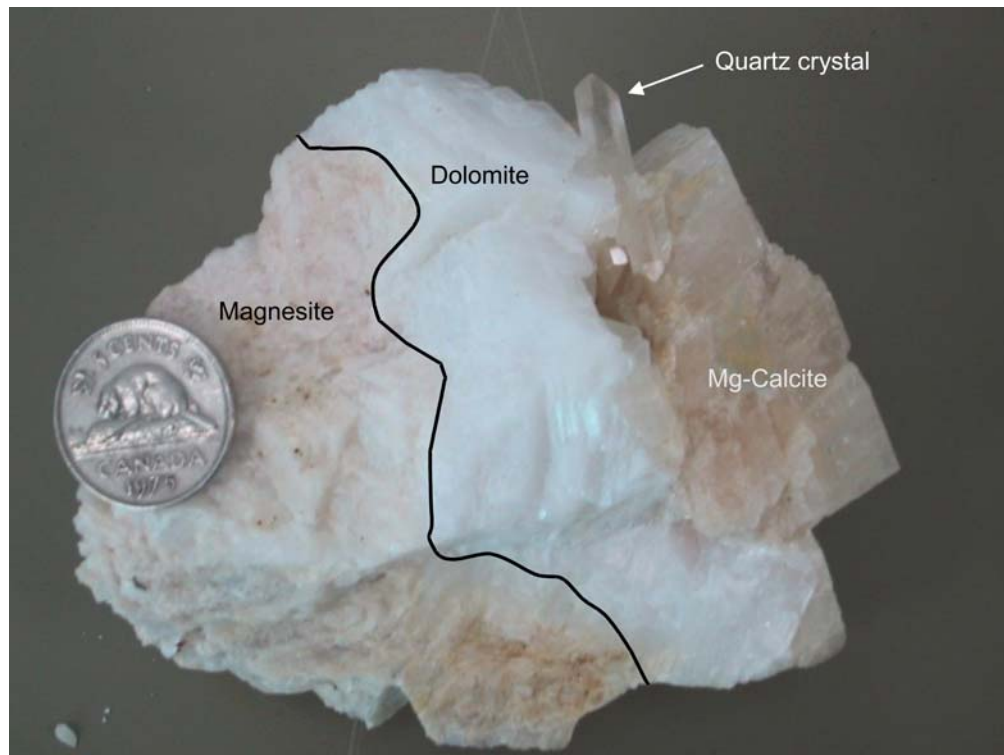


Figure 4. Quartz-carbonate fracture filling in magnesite. The central vein consists of quartz crystals in vug and vein-like settings. There is a white halo of dolomite forming a fairly sharp boundary with the magnesite host-rock. 5-cent coin for scale.

DISCUSSION

Both Type 1 and Type 2 fluid inclusions display total homogenization (Figure 10) to the liquid phase. This negates the possibility that the two fluids are conjugates of a boiling (immiscible) system, therefore boiling should not be considered as a possible mechanism for ore genesis in the Mt. Brussilof deposit. As has been shown, the two fluids more likely coexisted within the Mt. Brussilof rocks but originated from different sources. The compositions of fluid inclusions can be used to calculate minimum and maximum isochores for each fluid inclusion population. Isochores for the fluid inclusions in magnesite have been calculated using the equation of state of $H_2O-NaCl$ (Zhang and Frantz, 1987) and those representing the fluid inclusions in the quartz-carbonate veins have been calculated using the Bowers and Helgeson (1983) equation of state for $H_2O-NaCl-CO_2$. These isochores are shown on Figure 11.

Due to petrographic and field relations, Type 1 and Type 2 fluids are deemed to have coexisted in pressure-temperature space at the time of fluid inclusion trapping. This provides a unique opportunity to derive pressure-temperature constraints using the intersection of the isochoric limits obtained from the two fluid inclusion populations, which represent a non-boiling but probably mixed fluid system. As can be seen from

figure 11, the fluid inclusion isochoric data do not constrain lower temperature and pressure limits of the two fluid types. The lower pressure-temperature constraints are derived from the minimum (total) *homogenization* temperatures and pressures along the liquid vapour curve for $H_2O-NaCl$. This yields a minimum temperature limit of approximately $195^\circ C$ and a corresponding minimum pressure constraint of about 10 bars (Fisher, 1976). The maximum limit can be obtained where the two isochores diverge at higher pressure and temperatures (Figure 11). This places the maximum pressure and temperature estimates at 2650 bars and $305^\circ C$, respectively. Based on this data, the maximum burial depth of the Mt. Brussilof deposit was approximately 8 kilometres, which is consistent with the current tectonic models for the Cordillera (Wheeler and McFeely, 1991)

SUMMARY

Previous studies described the geological setting of the Mount Brussilof deposit and textural features compatible with either sedimentary, late diagenetic or hydrothermal origin (Simandl *et al.*, 1991; Simandl and Hancock, 1991 and 1999). The present study confirms that magnesite may have formed from Mg-rich magnesite precursors of sedimentary origin and that

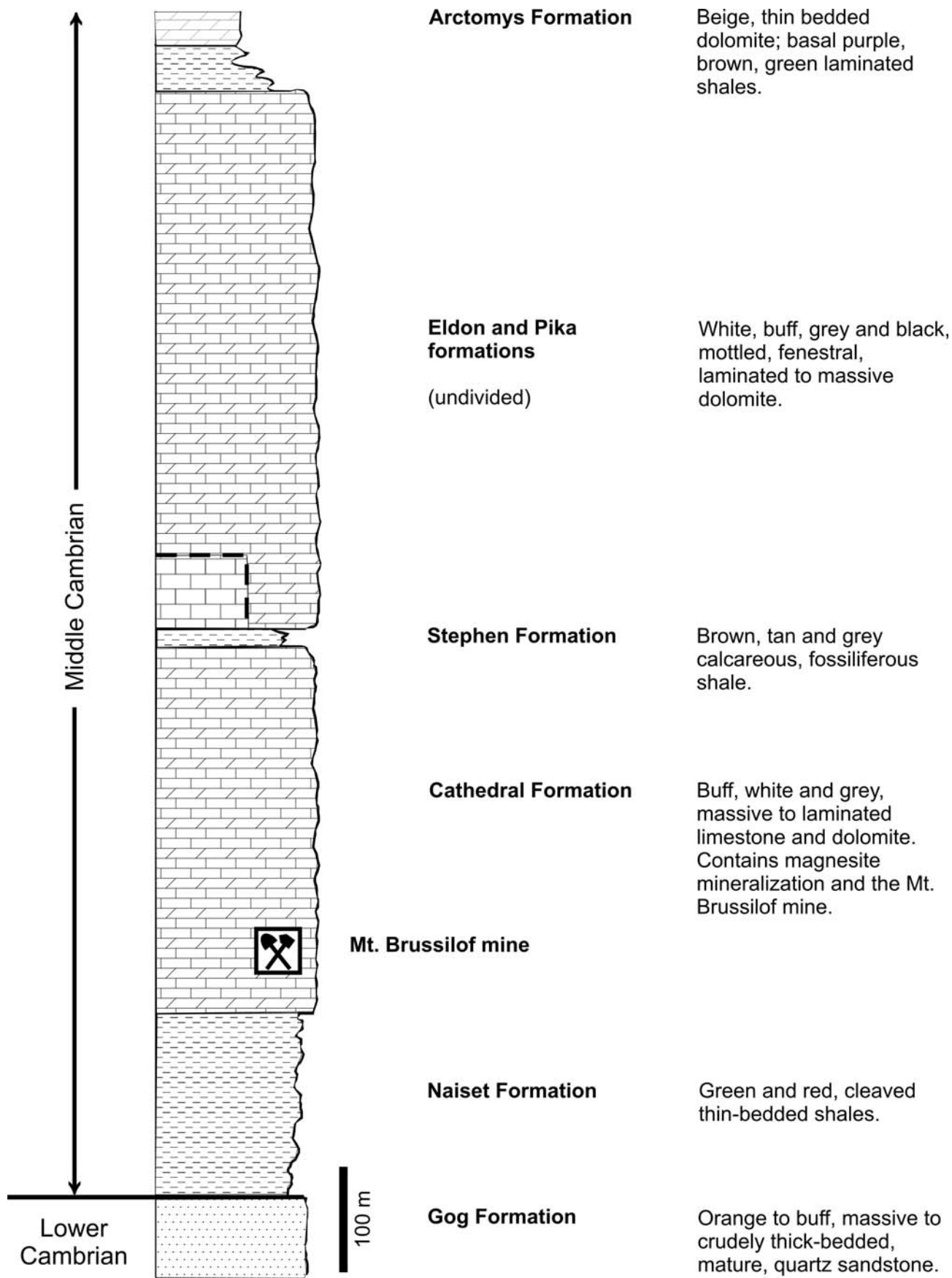


Figure 5. Stratigraphic column from the Mount Brussilof area (after Simandl, 1991)

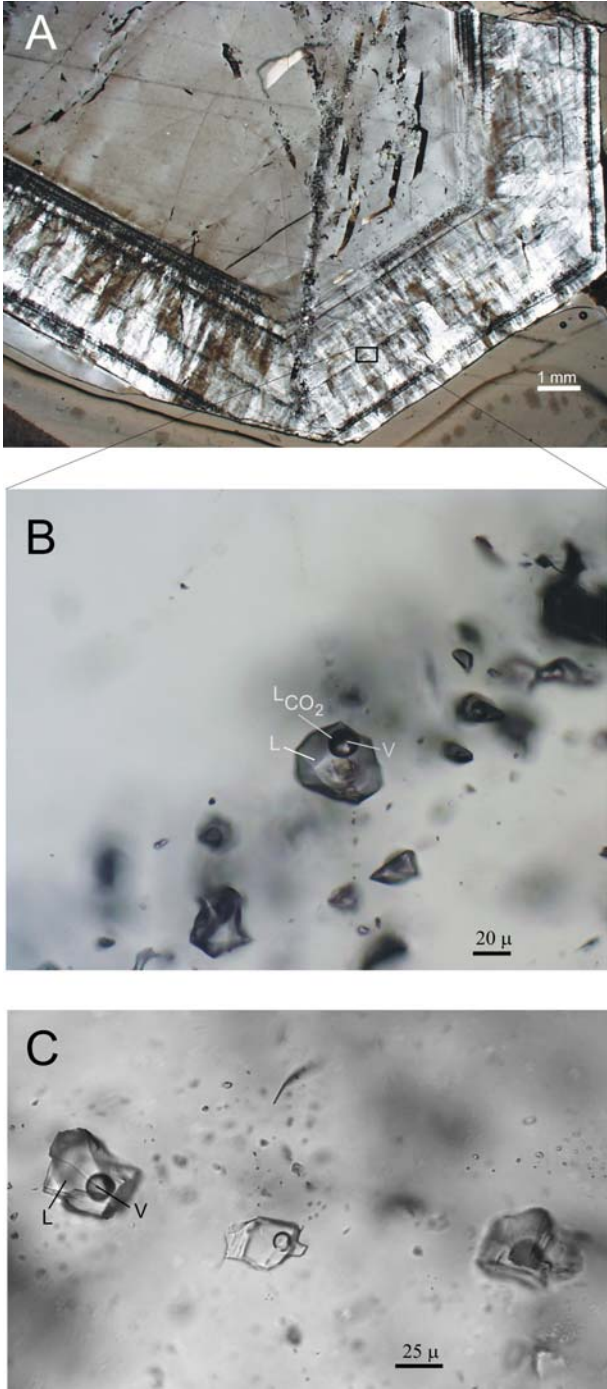


Figure 6. Photomicrographs. A: Zoned quartz crystal similar to that shown in Figure 5; B: Enlargement of the rectangle shown in photomicrograph A. The growth zones are delineated by linear arrays of fluid inclusions. These inclusions comprise three phases at room temperatures, CO₂ vapour (V), Saline brine (L), and liquid CO₂ (L-CO₂); C: Two phase fluid inclusions in dolomite at room temperature comprised of a saline brine (L) and a water vapour (V).

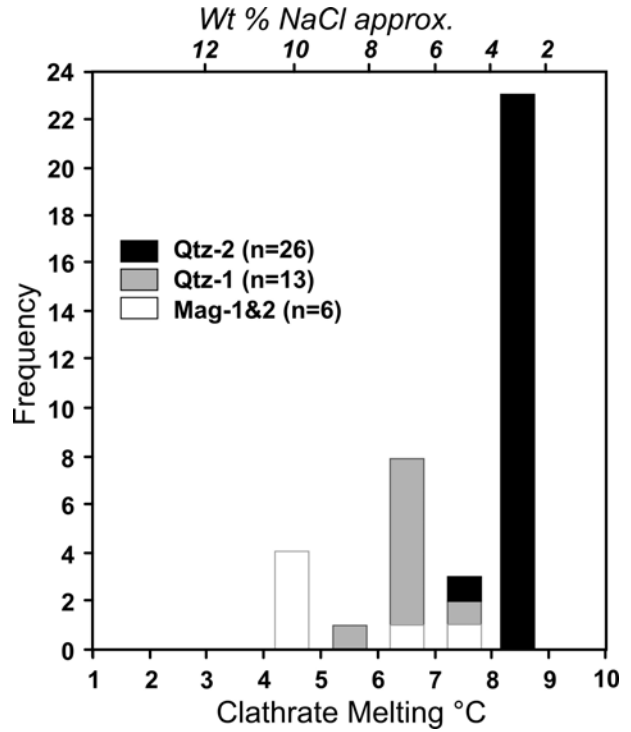


Figure 7. Clathrate melting histogram for the three-phase CO₂-bearing fluid inclusions in quartz and dolomite. Qtz: quartz data, Dol: dolomite data, n: number of measurements.

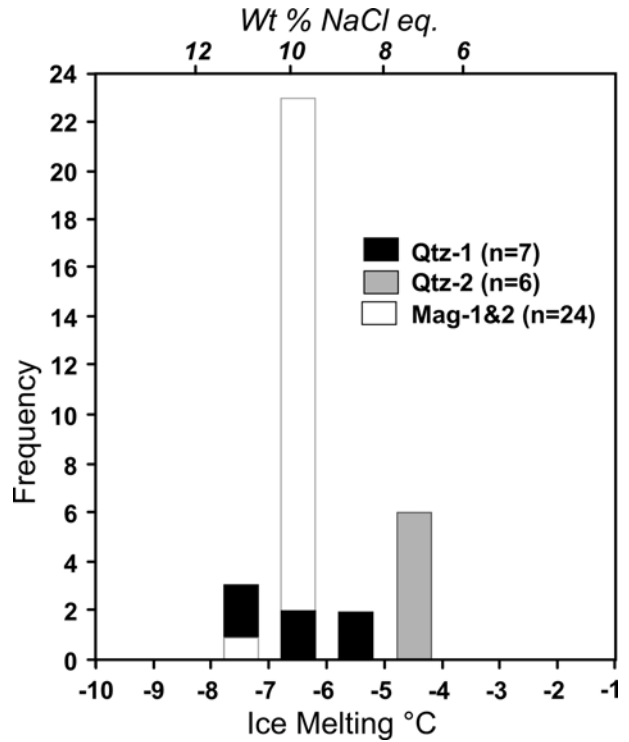


Figure 8. Ice Melting histogram of the microthermometric data from the two-phase inclusions in dolomite and quartz.

TABLE 1. MICROTHERMOMETRIC DATA FOR FLUID INCLUSIONS HOSTED IN QUARTZ CRYSTALS

Sample #	TM _{CO2}	TE	TM _{ice}	TM _{da}	TH _{CO2-v}	TH _{tot}	Sample #	TM _{CO2}	TE	TM _{ice}	TM _{da}	TH _{CO2-v}	TH _{tot}
Qtz-1-1		-45	-6.6	6		199	Qtz-2-1	-56.0	-29	-4.2	8.9		208
2			-0.8	6		195	2	-56.8	-20	-4.8	8.3	28.2	s 203
3			-3.5			s	3		-30	-4.9	8.3	29.2	s 204
4	-60	-23	-8.2	7.2		s	4	-56.5	-27	-4.7	8.3		
5			-5.3	6.4		190	5	-56.3	-29	-5.0	8.3	29.3	206
6			-6.4	6.7		214	6n	-56.6	-27	-5.0	7.5	29.8	210
7			-5.8	6.8		201	7	-56.7	-20	-4.6	8.6	28.9	206
8	-57	-33	-6.0	7.2	26		8	-56.5	-27	-4.9	8.3	28.9	208
9			-6.5				9	-56.5	-26	-4.8	8.3	28.8	208
10		-23	-5.6				10		-4.9	-4.9			191
11		-18	-5.8	5.1	26.1		11		-4.7	-4.7			192
11b		-27	-5.7	6.8			12		-23	-4.8			194
12		-24	-7.8				13		-20	-4.4	8.5		s
13		-38	-7.9				14a		-17	-4.8			199
14		-17	-4.6				14b		-17	-4.0			140
15		-20	-6.2	6.1			14c		-17	-4.2			186
16		-38	-8.8				15	-55.7	-17	-5.1	8.3	28.8	
17		-25	-7.9	6.7			16	-55.7	-18	-4.9	8.2	29.1	
18		-19	-8.2				17	-55.7	-30	-4.8	8.3	29.5	
19		-20	-6.0				18	-56.0	-31	-4.6	8.4	28.7	
20		-23	-5.0				19a		-17	-4.6	8.4		
21		-22	-6.9				19b		-17	-4.8	8.4		
22	-58.6	-23	-8.3				19c		-17	-4.9	8.3		
23			-7.8				20	-55.7	-17	-5.1	8.1	29.2	
24		-21	-7.0				21	-55.4	-18	-4.7	8.4	28.0	
25		-34	-6.8				22		-17	-4.6	8.4		
26			-7.5				23		-17	-4.8	8.2		
27		-27	-7.3				24		-20	-4.3	8.5	28.4	
28			-7.3				25		-18	-4.4	8.5	28.9	
29		-27	-7.6				26	-55.7	-17	-4.9	8.3	29.2	

TM = Melting temperature, TH = Homogenization temperature, TE = Eutectic temperature, V = vapour, all temperatures in °C, S = stretched, N = necked down, CLA = Clathrate

TABLE 2. MICROTHERMOMETRIC DATA FOR FLUID INCLUSIONS HOSTED IN MAGNESITE

SAMPLE #	TE	TM _{ICE}	TM _{CLA}	TH _{TOT}	SAMPLE #	TE	TM _{ICE}	TM _{CLA}	TH _{TOT}
MAG-1-1	-20	-4.9		133	MAG-2-1	-27	-6.0		
2	-25	-4.8		L >200	2	-17	-4.8		
3	-30	-4.8		188	3	-21	-6.6		
4	-17	-4.8		S	4	-30	-5.9		
5	-35	-4.7		S	5	-22	-6.8		
6	-18	-4.7		176.6	6	-27	-6.8		
7	-30	-4.9		>200	7		-6.5		
8	-20	-4.0		>200	8	-27	-5.3	7.9	
9	-14	-6.4		309	9	-27	-6.1		
10	-16	-6.4			10	-31	-6.7		
11	-21	-6.5		D	11		-6.7		
12	-21	-5.1			12		-6.8		
13	-24	-5.8		D	13	-20	-6.8		
14	-20	-5.6			14		-6.8		
15		-5.2		D	15	-15	-4.2		
16	-24	-5.2		297	16	-29	-6.8		
17		-4.5		D	17	-26	-6.2		
18	-16	-6.0		D	18	-25	-6.3		
19	-16	-6.0		276	19	-23	-6.7		
20	-19	-6.0		238	20	-31	-6.6		
21	-22	-6.1		D 341	21	-27	-6.6		
22	-28	-5.0		286	22	-18	-6.5	4.8	
23	-22	-4.4		D	23	-17	-6.5	4.8	
24	-22	-4.5		D	24	-20	-6.5	4.9	
25	-21	-4.7		D	25	-18	-6.4		
26	-25	-4.5		D	26	-15	-6.5		
27	-28	-4.3		D	27	-25	-6.4		
28	-28	-4.6		280	28	-16	-3.1		
29	-19	-7.3	6.7	D 305	29	-12	-2.8		
30			4.7		30	-22	-7.1		

TM = Melting temperature, TH = Homogenization temperature, TE = Eutectic temperature, all temperatures in °C, S = stretched, D = decrepitated, L = leaked, CLA = clathrate

these precursors may have been converted to sparry magnesite during diagenesis it also establishes the maximum pressure/temperature conditions for magnesite formation. Microscopic studies in at least one thin section identified textures indicating replacement of sparry dolomite by magnesite. The volume of this late hydrothermal magnesite (which post-dates sparry dolomite) appears to be minimal compared to the volume of magnesite ore that is interpreted to pre-date sparry dolomite. Sparry dolomite is widely distributed through the area and it is probably genetically related to Mississippi Type Pb-Zn deposits that are known to occur in this area (Simandl *et al.*, 1991).

The two distinct, intersecting fluid inclusion populations identified in this study are consistent with a fluid system that has not boiled and also place pressure-temperature constraints on both hydrothermal conditions and the coeval emplacement of quartz-carbonate veins. These constraints yield potential maximum temperatures of magnesite formation of 305°C with a corresponding pressure maximum of 2650 bars, which indicates burial depths on the order of 8

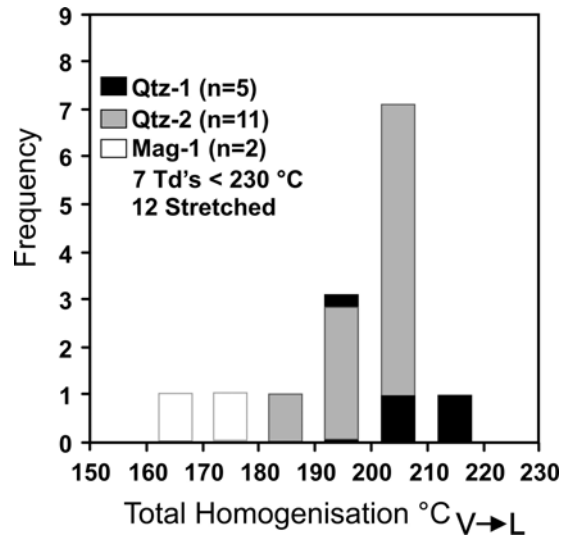


Figure 9. Total homogenization temperature histogram of the microthermometric data from the two-phase and three-phase fluid inclusions hosted within quartz and magnesite. All fluid inclusions measure homogenized to the liquid phase, with 7 inclusions decrepitating (Td) and 12 inclusions stretching. Data from the stretched and decrepitated fluid inclusions is not shown on the diagram.

kilometres. Minimum fluid inclusion homogenization temperatures of 195°C provide a minimum temperature limit of inclusion entrapment and diagenetic recrystallization or hydrothermal magnesite formation. Salinities of the magnesite-hosted two-phase fluid inclusions range from 6.4 to 7.8 wt% NaCl equivalent. Carbonic fluids responsible for emplacement of the quartz carbonate veins were not derived locally. They likely originated from an external source, suggesting nearby igneous or hydrothermal activity.

Exploration programs in southeastern British Columbia should be designed to be effective regardless of the origin of magnesite and compatible with both, the sedimentary/ diagenetic and hydrothermal hypotheses.

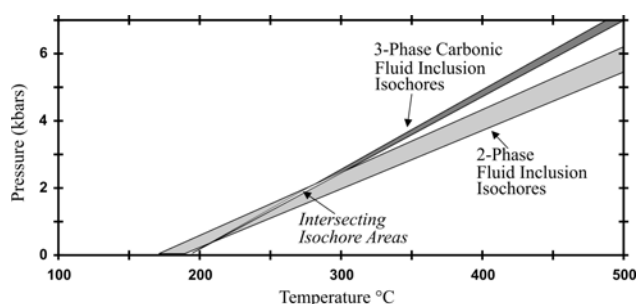


Figure 10. Pressure-temperature diagram showing the different isochoric constraints from the two fluid inclusion populations. The dark grey area represents the isochoric constraints derived from the three-phase carbonic fluid inclusions. The medium grey area portrays the constraints for the two-phase fluid inclusions. The light grey area represents the intersection of the two isochoric constraints.

REFERENCES

Aharon, P. (1988): A stable isotope study of magnesites from the Rum Jungle uranium field, Australia: Implications for the origin of strata-bound massive magnesites; *Chemical Geology*, Volume 69, pages 127-145.

Bowers, T.S. and Helgeson, H.C. (1983): Calculation of the thermodynamic and geochemical consequences of nonideal mixing in the system H_2O-CO_2-NaCl on phase relations in geologic systems: Equation of state for H_2O-CO_2-NaCl fluids at high pressures and temperatures; *Geochimica Cosmochimica Acta*, Volume 47, pages 1247-1275.

Fallick, A.E., Ilich, M. and Russell, M. (1991): A stable isotope study of the magnesite deposits associated with the Alpine-type ultramafic rocks of Yugoslavia; *Economic Geology*, Volume 86, pages 847-861.

Frtiz, W.H. and Simandl, G.J. (1993): New Middle Cambrian fossil and geological data from the Brussilof Magnesite Mine area, southeastern British Columbia; Current Research, Part A; *Geological Survey of Canada*, Paper 93-1A, pages 183-190.

Halfon, J. and Marce, A. (1975): Compositions isotopiques en carbon et oxygène de la magnésite de Serre de Motner et

autres carbonates associés dans la série de Canaveilles (Pyrénées-orientales): Conséquences génétiques; *Compte Rendus de l'Académie des Sciences de Paris*, Volume 290, pages 1521-1524.

Haas, J.L. Jr. (1971): The effect of salinity on the maximum thermal gradient of a hydrothermal system at hydrostatic pressure; *Economic Geology*, Volume 66, pages 940-946.

Kralik, M. and Hoefs, J. (1978): Die isotopensusammensetzung der karbonate in der magnesitlagerstätte Eugui (Westpyrenäen); *Tschermaks Mineralogische und Petrographische Mitteilungen*, Volume 25, pages 185-193.

Leech, G.B. (1965): Kananaskis Lakes, W. Area; Report of Activities, May to October, 1965, *Geological Survey of Canada*, Paper 66-1, pages 65-66.

Leech, G.B. (1966): Kananaskis Lakes; *Geological Survey of Canada*, Open File 634, map.

Lugli, S., Torres-Ruiz, J., Garuti, G. and Olmedo, F. (2000): Petrography and geochemistry of the Eugui magnesite deposit (Western Pyrenees, Spain): Evidence for the development of a peculiar zebra banding by dolomite replacement; *Economic Geology*, Volume 95, pages 1775-1791.

Moreani, G., Möller, P. and Schley, F. (1982): The rare earth element contents and the origin of sparry magnesite mineralizations of the Tux-Lanersbach Entachen Alm, Spiessnägel, and Hochfilzen, Austria and the lacustrine magnesite deposits of Aiani-Kozani, Greece and Bela Stena, Yugoslavia; *Economic Geology*, Volume 77, pages 617-631.

Pohl, W. (1990): Genesis of magnesite deposits - models and trends; *Geologische Rundschau*, Volume 79, pages 291-299.

Pohl, W. and Siegl, W. (1986): Sediment-hosted magnesite deposits; In: K.H. Wolf, Editor, Handbook of strata-bound and stratiform ore deposits, *Elsevier*, Amsterdam, Volume 14, pages 223-310.

Simandl, G.J. and Hancock, K.D. (1991): Geology of the Mount Brussilof magnesite deposit, southeastern British Columbia; Geological Fieldwork 1998, *British Columbia Ministry of Energy and Mines*, Paper 99-1, pages 269-278.

Simandl, G.J. and Hancock, K.D. (1992): Geology of dolomite-hosted magnesite deposits of the Brisco and Driftwood Creek areas, British Columbia; Geological Fieldwork 1991, *British Columbia Ministry of Energy and Mines*, Paper 99-2, pages 461-478.

Simandl, G.J. and Hancock, K.D. (1996): Magnesite in British Columbia, Canada: a neglected resource; *Mineral Industry International*, No. 1030, pages 33-44.

Simandl, G.J. and Hancock, K.D. (1999): Sparry Magnesite; In Selected British Columbia Mineral Deposit Profiles, Volume 3, Industrial Minerals and Gemstones, G.J. Simandl, Z.D. Hora and D.V. Lefebure, Editors, *British Columbia Ministry of Energy and Mines*, pages 39-41.

Simandl, G.J., Hancock, K.D., Hora, D.Z., MacLean, M.A. and Paradis, S. (1991): Regional geology of the Mount Brussilof carbonate-hosted magnesite deposit, southeastern British Columbia, Canada. In: Industrial Minerals of Alberta and British Columbia, Canada;

Proceedings of the 27th Forum on the Geology of Industrial Minerals; Z.D. Hora, W.N. Hamilton, B. Grant and P.D. Kelly, Editors, *British Columbia Ministry of Energy, Mines and Petroleum Resources*; Open File 1991-23, pages 57-65.

- Simandl, G.J. (2002): Chemical Characteristics and Development Potential of Magnesite Deposits in British Columbia, Canada. *In: Industrial Minerals and Extractive Industry Geology.*; P.W. Scott and C.M. Bristow, Editors; The Geological Society Publishing, London, UK, pages 169-178.
- Singh, K., and Sharma, R. (1997): Magnesite mineralization along the Chamba Thrust, Himachal Himalaya; structural control and depositional environment using fluid inclusions; *Journal of the Geological Society of India*, Vol. 49, No. 3, pages 289-296.
- Wheeler, J.O. and McFeely, P. (1991): Tectonic assemblage map of the Canadian Cordillera and adjacent parts of the United States of America; *Geological Survey of Canada*, Map 1712A. Scale 1:2 000 000.
- Zhang, Y.G., and Frantz, J.D. (1987): Determination of the homogenisation temperatures and densities of supercritical fluids in the system NaCl-KCl-CaCl₂-H₂O using synthetic fluid inclusions; *Chemical Geology*, Volume 64, pages 335-350.